

Durham Research Online

Deposited in DRO:

15 May 2020

Version of attached file:

Accepted Version

Peer-review status of attached file:

Peer-reviewed

Citation for published item:

Wang, Zhiwen and Xu, Jingping and Talling, Peter J. and Cartigny, Matthieu J.B. and Simmons, Stephen M. and Gwiazda, Roberto and Paull, Charles K. and Maier, Katherine L. and Parsons, Daniel R. (2020) 'Direct evidence of a high-concentration basal layer in a submarine turbidity current.', *Deep sea research part I: oceanographic research papers.*, 161 . p. 103300.

Further information on publisher's website:

<https://doi.org/10.1016/j.dsr.2020.103300>

Publisher's copyright statement:

© 2020 This manuscript version is made available under the CC-BY-NC-ND 4.0 license
<http://creativecommons.org/licenses/by-nc-nd/4.0/>

Additional information:

Use policy

The full-text may be used and/or reproduced, and given to third parties in any format or medium, without prior permission or charge, for personal research or study, educational, or not-for-profit purposes provided that:

- a full bibliographic reference is made to the original source
- a [link](#) is made to the metadata record in DRO
- the full-text is not changed in any way

The full-text must not be sold in any format or medium without the formal permission of the copyright holders.

Please consult the [full DRO policy](#) for further details.

Direct evidence of a high-concentration basal layer in a submarine turbidity current

Zhiwen Wang¹, Jingping Xu^{2,3}, Peter J. Talling⁴, Matthieu J.B. Cartigny⁴, Stephen M. Simmons⁵, Roberto Gwiazda⁶, Charles K. Paull⁶, Katherine L. Maier⁷, Daniel R. Parsons⁵,

¹College of Marine and Geosciences, Ocean University of China, 238 Songling Rd., Qingdao, Shandong, China, 266100

²Department of Ocean Science and Engineering, Southern University of Science and Technology, 1088 Xueyuan Rd., Shenzhen, Guangdong, China, 518055

³Laboratory for Marine Geology, Qingdao National Laboratory for Marine Science and Technology, Qingdao, Shandong, China, 266061

⁴Department of Earth Sciences and Geography, University of Durham, South Road, Durham DH1 3LE, United Kingdom

⁵Department of Geography, Environment and Earth Sciences, University of Hull, Cottingham Road, Hull HU6 7RX, United Kingdom

⁶Monterey Bay Aquarium Research Institute, 7700 Sandholdt Rd., Moss Landing, CA 95039, USA

⁷Pacific Coastal and Marine Science Center, U.S. Geological Survey, 2885 Mission St., Santa Cruz, CA 95060, USA

Corresponding author: Jingping Xu (xujp@sustech.edu.cn)

Abstract

Submarine turbidity currents are one of the most important sediment transfer processes on earth. Yet the fundamental nature of turbidity currents is still debated; especially whether they are entirely dilute and turbulent, or a thin and dense basal layer drives the flow. This major knowledge gap is mainly due to a near-complete lack of direct measurements of sediment concentration within active submarine flows. Here we present the most detailed near-bed sediment concentrations measurements from a powerful turbidity current in Monterey Canyon, offshore California. We employ a novel approach using correlations between conductivity and sediment concentration, which unlike previous methods can measure very high concentrations and not sensitive to grain size. We find that sediment concentrations close to the canyon floor gradually increased after the arrival of the turbidity current, until reaching a maximum value of 12%, the highest concentration ever inferred from direct measurements in turbidity currents. We also show a two-layer flow head, with a fast (up to 4 m/s), thin and dense basal layer overlain by a thicker (~50 m) dilute flow. At the interface of these two layers, there seems to be a sharp steep concentration gradient. Such quantitative measurements of sediment concentration can produce a key step forward in understanding the basic character and dynamics of these powerful submarine flows.

Keywords: Turbidity currents; Sediment concentration; Seawater conductivity; Monterey canyon

1 Introduction

Whether high sediment concentration layers occur at the base of turbidity currents has long been debated (Kuenen and Migliorini, 1950; Middleton, 1967; Lowe, 1982; Postma et al.,

1988; LeClair and Arnott, 2003; Talling et al., 2012). The controversy mainly focuses on whether these submarine flows are entirely dilute ($\ll 1\text{-}2\%$ by volume) and fully turbulent, perhaps with a bedload layer just a few grains thick (as is the case for almost all rivers), or whether a dilute layer overlies a much denser ($\sim 10\text{-}40\%$), up to several meters thick basal layer that drives the flow (Kuenen and Migliorini, 1950; Sanders, 1965; Lowe, 1982; Middleton, 1993; Kneller and Branney, 1995; Talling et al., 2012). The fundamental differences between entirely dilute flows and flows with dense basal layers are very important because they control flow speed, runout, impact forces on seabed structures or cables, and how flows deposit sediment. This question is hard to answer using flow deposits or physical and mathematical modelling, as dense or dilute flows can potentially produce similar deposits (Talling et al., 2012), whilst initial flow density is a predefined input condition for modelling. Lack of direct measurements in full-scale submarine flows is one of the root causes of the debate.

More recently, rare field observations have provided limited evidence for the multiple layer structure that has been theoretically or experimentally predicted (Middleton, 1969; Garcia and Parker, 1993; Mulder and Alexander, 2001). Hughes Clarke (2016) used multibeam sonars to show a thin ($< 2\text{ m}$) layer of higher sediment concentration within flows at Squamish Delta in British Columbia, and this dense basal layer caused up-slope migration of bedforms. Based on a multibeam sonar image of a turbidity current from the Scheldt River, Netherlands, Clare et al. (2015) observed a highly reflective basal layer underlying a more dilute layer. However, these field studies were unable to quantify the density of the basal layers due to lack of direct measurements. Quantifying sediment concentration in the field thus remains a key challenge for understanding what turbidity currents are, and how they work (Bornhold et al., 1994; Clare et al., 2015; Talling et al., 2015, Stevenson et al., 2018).

64 This paper presents evidence of a high-concentration basal layer within a submarine
65 turbidity current in Monterey Canyon. Concentrations as high as 12% by volume were
66 determined innovatively by using a conductivity sensor.

67 We first describe a turbidity current that was recorded on 15 January 2016 by an array of
68 seven moorings and one Seafloor Instrument Node (Paull et al., 2018). This array, extending for
69 50 km along the canyon between 300 and 2000 m water depth (Figure 1), recorded the most
70 detailed measurements yet of submarine turbidity currents. We then show experimental
71 calibrations between sediment concentration and conductivity, which allowed us to calculate
72 sediment concentrations in the basal layer recorded by the MS5 mooring at 1450 m water depth.
73 Finally, we interpret the field results, and discuss the wider implications for better understanding
74 turbidity currents.

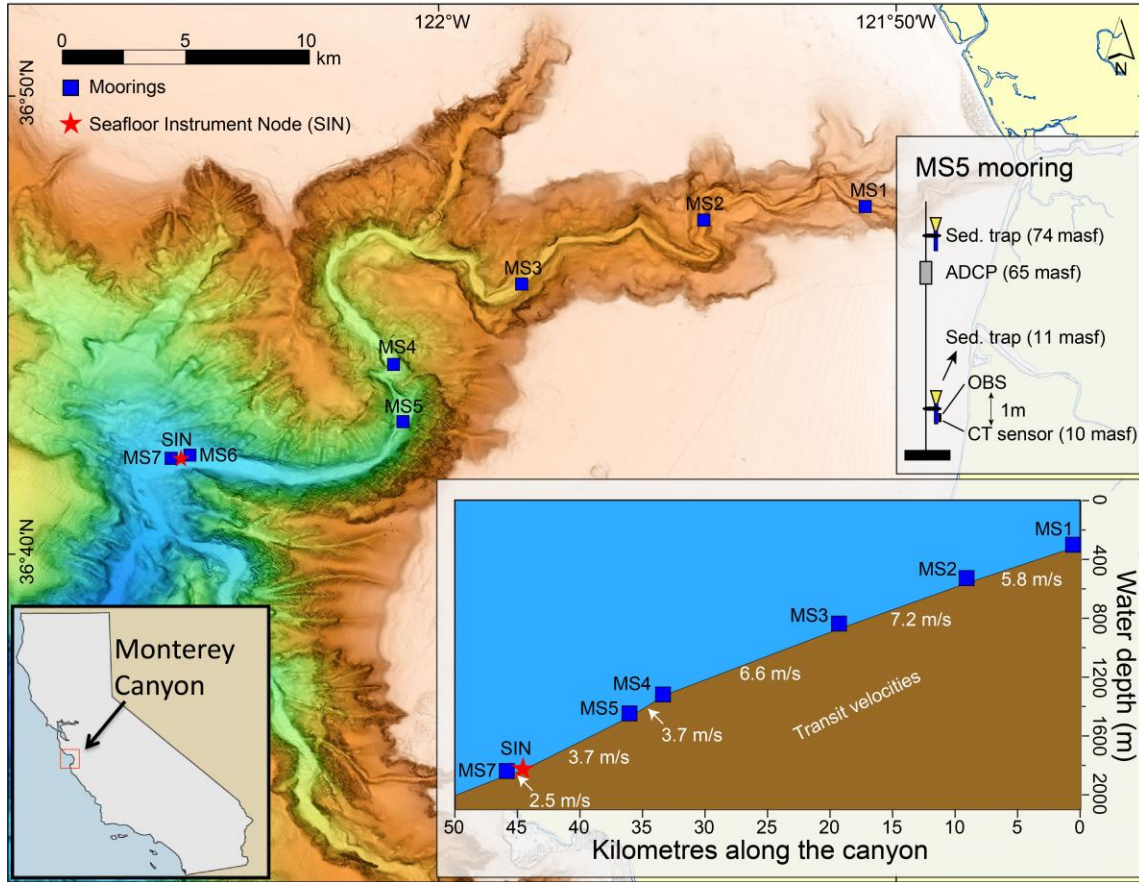


Figure 1. Location map of Monterey Canyon showing the seven moorings, and one seabed frame (SIN), along the submarine canyon. Axial bathymetric profile, with mooring sites, along the canyon are shown in the inset at the lower right. Transit velocities (white numbers) of the 15 January 2016 flow are calculated from distance along the canyon-floor thalweg, and difference in arrival time between moorings. The mooring configuration for MS5 is shown by the mooring conceptual diagram.

2 Turbidity Current Event on 15 January 2016

The turbidity current was recorded by 7 moorings (Figure 1) that were equipped with Acoustic Doppler Current Profiler (ADCP), Conductivity/Temperature (CT) sensors, optical backscatter sensors (OBS), and sediment traps. The general character of the flow was previously

reported by Paull et al. (2018). And in this study, we only focus the data of the mooring at 1450 m (MS5), the RBR[®] CT sensor on which recorded a conductivity anomaly during the event that allowed us to apply a novel approach of quantifying the super-high sediment concentration. The initial thickness of the flow estimated by the ADCP was about 20 m (Figure 2A). Thus, CT sensor mounted 10 meters above sea floor (masf) and OBS mounted 11 masf were well inside the body of the flow (Figure 1). At the arrival of the flow, the measured turbidity increased very quickly to reach a peak value of over 800 NTU (nephelometric turbidity units) before gradually returning to pre-event level (Figure 2C). At the same time, the measured conductivity of turbidity current rapidly decreased, by as much as 30%, before it gradually returned to pre-event values over the next three and a half hours (Figure 2D). Temperature increased by as much as 1°C during the same period. The transit velocities of the flow ranged between 2.5 and 7.2 m/s, and averaged 5.4 m/s for the stretch of the canyon occupied by the mooring array (Paull et al., 2018; Figure 1). The maximum instantaneous velocity measured by the MS5 ADCP was 4.1 m/s (Paull et al., 2018), and the transit speed here is 3.7 m/s (Figure 1). They are by far the fastest velocities directly measured by moored sensors in submarine flows (Xu et al., 2004, 2014). The entire turbidity current lasted about 6 hours (Figures 2A and 2B).

Two sediment traps on MS5, at 11 and 74 masf, collected sediment in the flow (Figure 1). The lower trap contains coarser sand than the upper sediment trap (Maier et al., 2019). Because the thickness of the flow is much less than 70 m, judging from the ADCP measured flow structure, sand in the upper trap either came from the billows in the flow or clouds that arrived after the main body of the flow, or the trap was pulled closer to the sea bed (Paull et al., 2018).

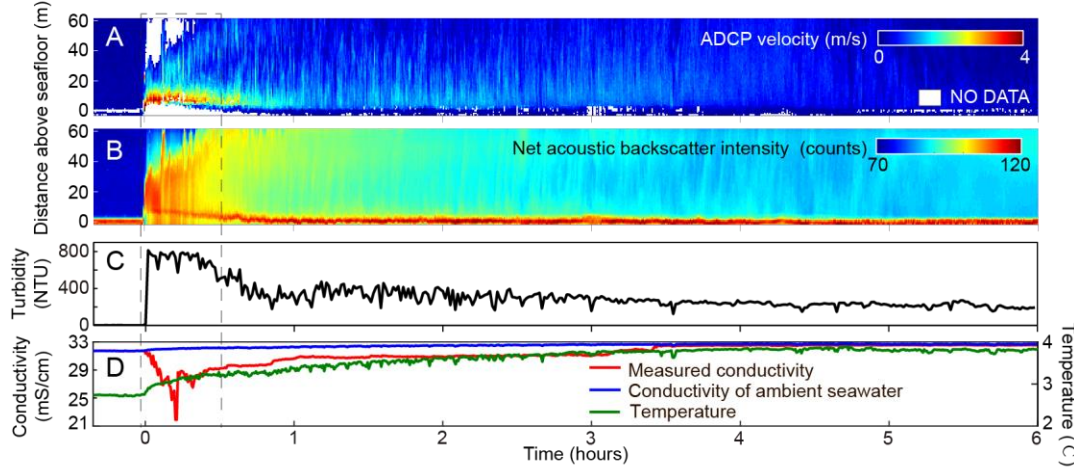


Figure 2. Velocity and echo intensity during 15 January 2016 flow event. A: Time series of flow speed measured by a downward-looking ADCP initially mounted 65 meters above sea floor (masf). B: Time series of net acoustic backscatter intensity (averaged over four beams) measured by the ADCP; the influence of water attenuation and spherical spreading have been corrected. C: Time-series of water turbidity measured by OBS initially mounted at 11 masf. D: Time series of temperature (green) and conductivity (red) measured by CT sensor initially mounted at 10 masf. Conductivity of ambient seawater (blue) was calculated using a standard formula (Poisson, 1980) by assuming a constant salinity.

3 Conductivity Anomaly and Sediment Concentration Calculations

3.1 Cause of the conductivity anomaly

The most common and direct cause of conductivity decrease is addition of freshwater. Assuming this is the case for the conductivity anomaly shown in Figure 2D, the volume of the added freshwater ($V_{freshwater}$) can be estimated by the salinity difference between the ambient seawater ($S_{seawater}$) and the water mass inside the turbidity current ($S_{turbidity}$):

$$V_{freshwater} = V(S_{seawater} - S_{turbidity})/S_{seawater}, \quad (1)$$

where V is the volume of the turbid water mass that can be grossly estimated by simplifying the flow to a cuboid of 50 m (flow depth) \times 50 m (canyon width at the MS5 mooring site) \times flow length. The flow length can be obtained by multiplying the average flow speed and the duration of the peak flow. Such calculations show that it would require $4.6 \times 10^6 \text{ m}^3$ of freshwater in order to produce the observed conductivity anomaly at MS5. It is almost certain that influx of this much freshwater into the canyon was impossible because: 1) there was hardly any rainfall in the Monterey area during the week before the event; and 2) a sudden release of several millions of cubic meters of fresh groundwater is very unlikely. Thus, the freshwater cause of the conductivity anomaly can be ruled out, and the increase of the temperature (Figure 2D) during the flow was induced by the warmer seawater input from the upstream canyon.

Very high sediment content can also cause conductivity decrease because the conductivity of sediment grains is several orders of magnitude smaller than the conductivity of seawater (Traykovski et al., 2000). Applying Archie's law (Archie, 1942) that relates conductivity and volume sediment concentration, we obtain:

$$\frac{\gamma_{mixture}}{\gamma_{seawater}} = (1 - C_{sediment})^m, \quad (2)$$

where γ is the conductivity that can be measured by CT sensor, C is the volume concentration, and m is an empirical parameter that ranges from 1.2 to 3.0 (Jackson et al., 1978). Equation (2) would allow us to estimate the sediment concentration C if the constant m becomes known.

3.2 Laboratory experiments of estimating m

To quantify the relationship between conductivity and sediment concentration (Equation 2), a series of laboratory experiments were conducted to measure the variations of conductivity of sea-water and sediment mixtures under different combinations of sediment concentration and

temperature conditions. The experiment started with making a saline solution of 34-35‰ by dissolving table salt in a container (bucket#1) with 25 liters of tap water. Roughly 2 kg (dry weight) of sediment was poured into the saline solution while stirring vigorously to make a well-mixed slurry (Figure 3). An incremental scheme of measuring the conductivity of the sediment-water mixture was carried out as follows:

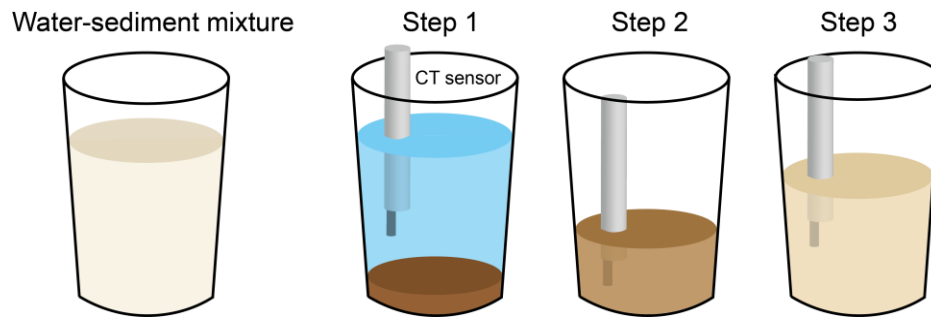


Figure 3. Interpretive diagram showing the experiment process.

1) After all sediment particles had completely settled on the bottom of bucket #1, the salinity, conductivity and temperature of the clear solution in the upper part of the bucket was measured with a RBR[®] CT sensor (the same type of instrument as used on the mooring during the January 15th flow).

2) About 80% of the clear water was removed from bucket#1 to another empty bucket (bucket#2). The remaining mixture of water and sediment in bucket#1 was vigorously stirred to a well-mixed state while continuously measuring the conductivity and temperature of the mixture with the same RBR[®] CT sensor. A sample of the sediment-water mixture was collected into a small jar for sediment concentration calculation using a drying and weighing method. This first sample had the highest concentration and the lowest conductivity value.

163 3) A small amount of the clear saline water from bucket#2 was added back to bucket#1,
164 vigorously stirred to a well-mixed suspension while continuously measuring the conductivity and
165 temperature. A sample was taken for sediment concentration determination.

166 4) Step 3 was repeated until all the clear saline water in bucket#2 was added back to the
167 mixture in bucket#1. This incremental dilution made the last sample the lowest sediment
168 concentration but the highest conductivity value.

169 Two types of sediment were used in the experiments: finer material (clay) with median
170 diameter of 0.03 mm collected from a mud flat, and coarser sediment (quartz sand) with median
171 diameter of 0.29 mm. Considering that the influence of the sediment content in the seawater to
172 the mixture's conductivity, depend on the ratio of sediment particles' conductivity to the
173 seawater conductivity. And the conductivity of sediment grains is always several orders of
174 magnitude smaller than the conductivity of seawater. Hence, the impacts of the mineralogy of the
175 sediment, which can only influence the absolute conductivity of the sediment grains, are rather
176 limited to the mixture's conductivity changes.

177 The experiments were conducted at room temperature (20-24°C) and in a refrigerated
178 environment (1-4°C). The same procedure (steps 1-4) was repeated for a total of 4 times: 2 grain
179 sizes (fine and coarse) and 2 temperatures (room temperature and refrigerated). The results of
180 these four experiments are listed in Table S1. As shown in Figure 4, the correlation coefficient is
181 0.94 when the empirical exponent m is 2. This suggests that Equation (2) can be used to calculate
182 the sediment concentration from measured conductivity, at least for the range of grain-sizes and
183 temperatures used in these calibration experiments.

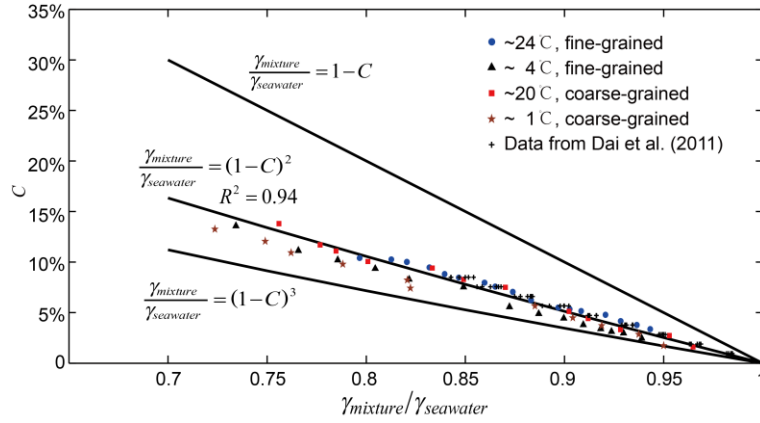


Figure 4. Plot of sediment volume concentration (C) against the conductivity ratio between the sediment-water mixture ($\gamma_{mixture}$) and seawater ($\gamma_{seawater}$). Symbols denote measurements from the four laboratory experiments and a previous calibration dataset from Dai et al. (2011). $\gamma_{mixture}$ was measured with 30 different combinations of environmental factors in Dai's experiment: 2 grain sizes (27 and 52 microns, median diameter), 3 salinities (22‰, 27‰, 32‰), and 5 temperatures (9.2°C, 10.2°C, 15.2°C, 19.2°C, 34.2°C). Solid lines are volume sediment concentrations derived using Equation (2), with $m = 1, 2$, and 3 respectively. $m = 2$ gives the best fit to experimental data.

3.3 Sediment concentration calculations

Assuming seawater salinity throughout the event was constant at the pre-event value (35.4‰), the conductivity of the ambient seawater in the turbidity current (Figure 2D) can be calculated using a standard formula (Poisson, 1980). The ratio between measured and ambient conductivities (Figure 2D) is then used to estimate sediment concentration of the first 30 minutes of the 15 January 2016 flow event (Figure 5A) by Equation (2), with $m = 2$. The rapid decrease of conductivity (i.e. increase of concentration) around minute 12 is believed to result from sensor

failure (clogged or partially clogged, see the discussion below for details), therefore the maximum valid concentration is 12% that was recorded at minute 11 (Figure 5A).

For comparison, ADCP acoustic backscatter and OBS outputs, both proxies for sediment concentration (Gartner, 2004; Ha et al., 2011), are plotted for the same 30 minutes time window after the arrival of the turbidity current (Figure 5B). It clearly shows that the 26 mS/cm conductivity (maximum sediment concentration) took place about 11 minutes after the arrival of the turbidity current that was marked by the rapid increase of both the ADCP backscatter and the OBS measurements (Figure 5). The measurements of OBS (located 1 m above the CT sensor), which are normally used in dilute flows for estimating sediment concentrations, shows the same pattern as vertically averaged ADCP backscatter (Figure 5B).

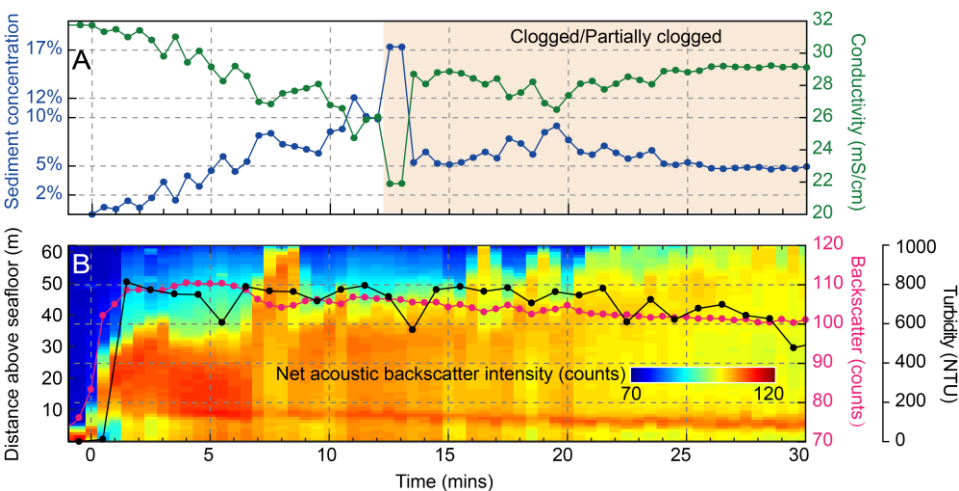


Figure 5. A: Sediment concentration (blue line) converted from the measured conductivity (green line) reduction for the first 30 minutes of 15 January 2016 flow event, using Equation (2), with $m = 2$. The shaded section after minute 12 indicates a clogged or partially clogged sensor. B: Close-up view of the net acoustic backscatter intensity (Figure 2B) for the first 30 minutes of the flow. Overlaid are the vertically averaged acoustic backscatter shown in the red line and the

OBS measurements in black. The flow thickness, necessary for the vertical averaging, is defined as: $h = (\int_0^z u dz)^2 / \int_0^z u^2 dz$, where z is the height above the bed, u is the flow speed.

4 Discussion

This paper describes a new and robust way of measuring high sediment concentrations, however, when used in turbidity currents, its limitation needs to be aware of. This method will not work in environments where the salinity changes appreciably, because we cannot distinguish whether the conductivity decrease in a flow is caused by sediment content or salinity variations. Hence, our approach assumes a constant seawater salinity of 35.4‰ throughout the 15 January 2016 flow event. If the salinity measured at the shallower mooring MS1 at 300 m water depth (34.1‰) was used instead for the ambient value, sediment concentration would have been overestimated by a maximum of 1.6 % volume. The actual error would be smaller because of entrainment of saltier water and turbulent diffusion of salt (Zhao et al., 2018) in the head of the flow as it travels down canyon.

4.1 Was the CT sensor clogged?

The inductive conductivity cell of the RBR[®] CT sensor is normally used to measure salinity by allowing seawater to flow freely through the 13 mm diameter hole (with a cross-section area of 1.33 cm²) in the center of the cell. In some extremely high concentration with coarse grains or clasts, such as near the bottom of turbidity currents, the hole could be clogged or partially clogged by gravel(s) or mud clast(s). Any clogging will reduce the effective cross-section area that will lead to a decrease of measured conductivity (Light et al., 1989).

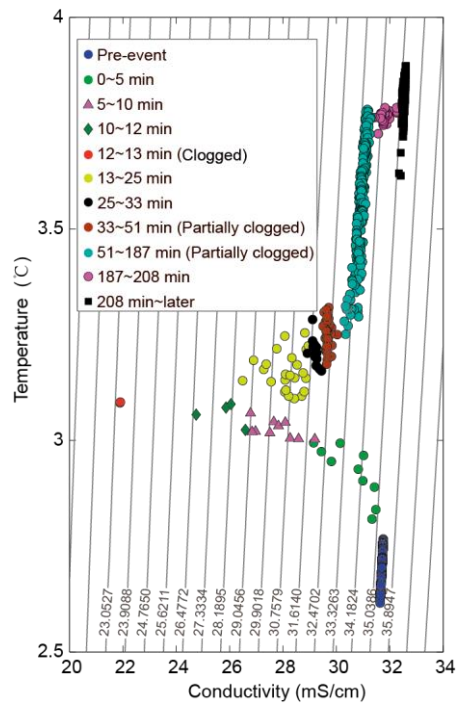


Figure 6. Temperature-conductivity plot of the 15 January 2016 turbidity current (green and red lines in Figure 2D). The measurements were separated into several segments. The thin, parallel lines are isohaline (units: ‰) computed using the formula in Poisson (1980).

The seawater temperature and conductivity at MS5 prior to the arrival of the turbidity current co-vary on a T-C plot along an isohaline corresponding to the ambient salinity of 35.4‰ (Figure 6). After the flow arrived (minute 0-12), the measured conductivity, now affected by the high sediment concentration in the flow, varies independently of measured temperature. Rapid decrease of conductivity between minutes 12 and 13 (Figure 5A) is almost identical to the response of the sensor in laboratory experiment when its cell was blocked by a piece of cardboard (Figure 7), suggesting that the sensor was clogged by coarser sediment or mud clasts. The recovery of the conductivity value from minutes 13 to 24 seems to indicate that the clogging was eased or even completely unclogged. If the latter is the case, it shows that the concentration hovered around 5% for another 11 minutes (Figure 5A). We are not confident about this because

there is no good explanation why the sensor became unclogged between minutes 13 and 24 before it was surely clogged again (see below).

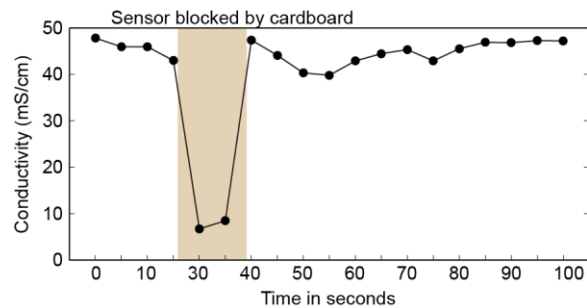


Figure 7. Conductivity readings of the CT sensor in a laboratory experiment with saline water of salinity of 33‰. When the hole of the CT sensor was blocked with a piece of cardboard, the conductivity reading rapidly decreased.

From minutes 25 to 33 (Figure 6), however, the measured conductivity and temperature co-varied parallel to an isohaline of much lower salinity (31.8‰). From minutes 33 to 51, the co-variation followed the isohaline of 32.2‰, and from minutes 51 to 187 followed the isohaline of 33.3‰. Noticeably both salinities are much lower than the salinity of 34.1‰ measured by a mooring near the head of the canyon. This unusual structure, where the conductivity is off by a fixed amount in each segment, is unlikely due to the high sediment concentration because (1) sediment concentration alone cannot induce the co-variation of conductivity and temperature, and (2) the near bed salinity at the mooring site should be no less than the salinity of the canyon head (34.1‰). Therefore, it is much more likely that the sensor was partially clogged, producing a ‘false’ signal of low conductivity.

All things considered, only the conductivity measurements in the first 12 minutes can be reliably used to estimate sediment concentrations of the turbidity current, which include the maximum concentration that we are confident is valid.

4.2 A two-layer system

If we apply a Chezy-type model (Bowen et al., 1984), the vertically-averaged concentration inside the flow had to be at least 9% (240 g/l) to maintain the depth-averaged velocity of the turbidity current body measured by the ADCP, assuming no momentum inherited from upslope. Such concentrations would be too high for acoustic penetration by ADCP according to previous studies (Thorne et al., 1993; Shen and Lemmin, 1996), yet the MS5 ADCP recorded valid data throughout the water during the event (Figure 5B). Hence, the high velocity in the flow is more likely due to the presence of a fast-moving, dense, basal-layer that dragged the overlying dilute flow from underneath, which is consistent with the turbidity current travelling model proposed by Paull et al. (2018) and Heerema et al. (2020) based on the movement of very heavy objects and self-acceleration of the flow.

To examine the vertical change of sediment concentration, calibrations were applied to convert the recorded OBS values from the engineering units (NTU, Figure 5B) to sediment concentration. For a given concentration, the OBS output was much more sensitive to fine sediments than to their coarse counterpart. For example, it requires a concentration of 2.5% of coarse sediment to produce the same OBS output of 1400 NTU that would only need a mere 0.1% concentration for the fine material (Figure 8). Hence, particle size must be determined when the OBS is used as an indirect measure of sediment concentration. According to the sediment collected at 11 masf during the turbidity current, the suspended sediment in the January 15 flow contained a wide range of grain sizes (Maier et al., 2019), the 600-800 NTU readings during the first 30 minutes (Figure 5B) could result from a variety of concentrations (Figure 8). However, the 600-800 NTU always represents a dilute flow with the sediment concentration no

more than ~1%, because the grain size of the sediment from the turbidity current (Maier et al., 2019) was well within the range of calibration experiments.

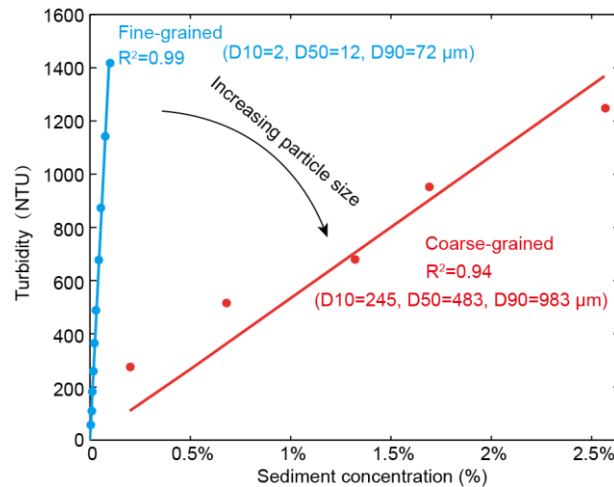


Figure 8. OBS output (NTU) versus sediment concentration from our laboratory experiments using fine (D50=12 microns) and coarse grained (D50=483 microns) natural sediments. Symbols denote measurements from the two experiments; solid lines are linear curve fitting.

These observations suggest that the 15 January 2016 turbidity current featured a two-layer structure, a dense basal layer whose concentration was as 12% or possibly higher, overlain by a dilute flow with concentration below 1.0%. Moreover, there seems to be a steep concentration gradient between the basal layer and upper dilute layer because 1) the OBS recorded a dilute flow during the event, 2) the recovered sediment trap showed no signs of strong abrasion as might be expected in a dense layer, and 3) parts of the flow imaged by the ADCP were also dilute (< 1%).

4.3 The 11 minutes delay of the CT measured concentration peak

The discrepancy between the CT-derived sediment concentration (gradual increase until the sensor was clogged at minute 12) and ADCP backscatter (rapid jump to maximum and then

gradually decline) is believed to have resulted from a combined effect of the two-layer structure of the flow, the mooring tilt due to the drag by the very fast flow and the bedform migration (or net deposition).

ADCPs measure vertical profiles of the entire water column below. The downward-looking MS5 ADCP recorded the arrival of the flow with a rapid increase of backscatter intensity. In contrast, the CT sensor only records parameters at the height where it is positioned. Moorings of similar design are prone to tilting (Symons et al., 2017), which can move both the ADCP and CT sensor toward the seafloor. We therefore have to determine how far the CT sensor and ADCP were pulled down towards the seabed.

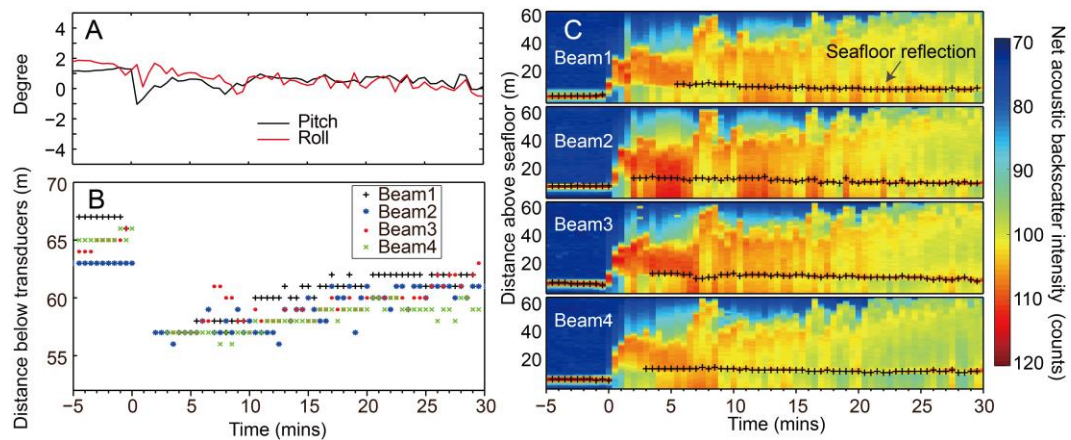


Figure 9. A: ADCP pitch and roll of MS5. B: Location of the highest magnitude acoustic backscatter for all four beams (Beam1~Beam4), which can be used to estimate the position of the seafloor (as shown in C). C: Net acoustic backscatter intensity profiles of individual beams during the first 30 minutes of the flow, the plus signs denote the position of the seafloor echoes

Maximum echo intensity of the backscatter signal from the ADCP can be used to estimate the position of the seafloor. The pre-event seabed position was used as the reference for the ADCP profiles. Figure 9C shows the highest magnitude acoustic backscatter for all four

beams (Beam1~Beam4). However, during the first 2 minutes of the flow, the ADCP cannot penetrate the high concentrated flow and get clear seafloor echoes, which makes it impossible to estimate the seabed position. But after minute 2, the distance from the ADCP to seafloor was several meters less than its pre-event value (Figure 9B). This could be due to tilting of the mooring by the fast flow, bed aggradation, or both. The pitch and roll (Figure 9A) showed only a very slight wobble when the flow hit the mooring, and the maximum tilt angle of the ADCP was < 2 degrees, which would increase the range to the seafloor by less than ~ 4 cm. Hence, the ADCP itself is nearly straight when the lower part of the mooring was severely tilted by the flow. The CT sensor was thus estimated to be ~ 8 m lower than its initial height (10 masf), with an actual height of ~ 2 masf after the arrival of the flow (minute 2), and gradually rose to ~ 6 masf at minute 30 (Figure 9B, Figure 10). Because of the assumptions to this approach, these estimated values of sensor's height are not exact, despite the fact that the CT sensor did experience a sharp deepening at the arrival of the flow, before gradually returning to the pre-event position.

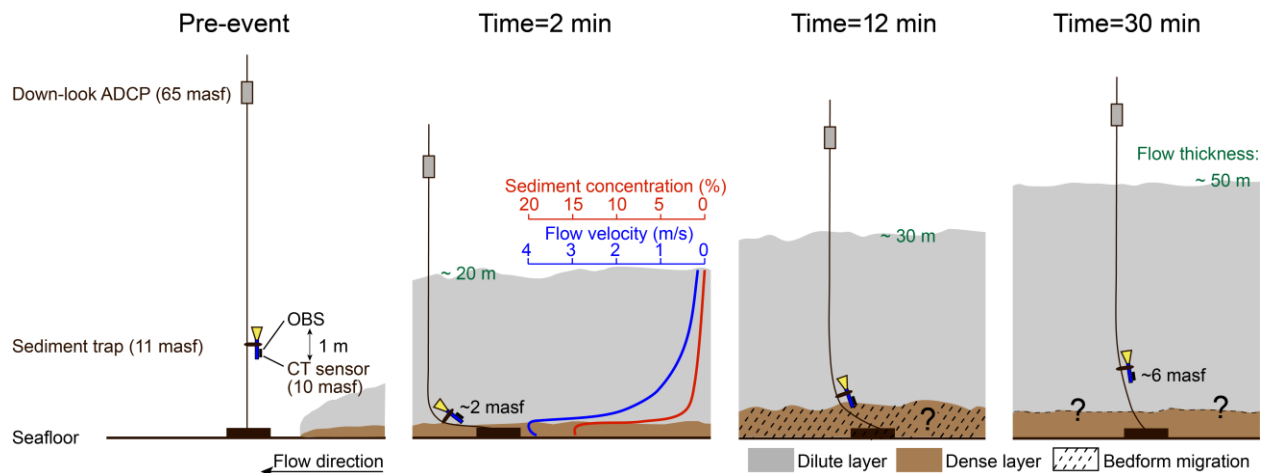


Figure 10. A conceptual diagram of mooring movement and the two-layer structure of the 15 January 2016 turbidity current, inferred from instruments layout on the mooring, ADCP pitch

and roll, and the position of the seafloor. The blue and red lines denote the conceptual velocity and concentration profiles within the flow at around 2 minutes after the arrival of the flow.

Considering that the mooring didn't moved during the Jan 15 turbidity current because 1) the slight of ADCP sway (pitch and roll) when the flow hits the mooring (Figure 9A), indicating that the mooring didn't experience a hydrodynamic drag on the upper ADCP and floats which would cause the mooring to slant backwards as the anchor moved more rapidly at the base, 2) the ADCP range to seafloor before and after Jan 15 event showed a same bedform (Figure S1). The bathymetric difference of the ADCP beam footprint on seafloor was thus obtained by comparing the distance from the ADCP to seafloor before and after the 15 January 2016 turbidity current (Figure 11), which shows similar magnitudes ($\pm 3\text{m}$) of both erosion and deposition on the circle with $\sim 25\text{ m}$ radius. It seems to show a blue 'trough' (closer to the center) and a red 'crest', both perpendicular to the flow direction, suggesting the presence of a bedform downstream from the mooring, roughly where the sediment trap was pulled down toward the seafloor.

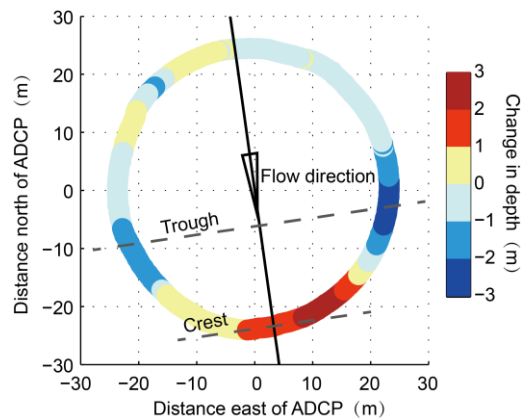


Figure 11. Bathymetric difference of the ADCP beam footprint on seafloor before and after 15 January 2016 turbidity current.

Based on the above analyses and the velocity measurements by ADCP, the flow can be inferred to have a two-layer structure with a fast (up to 4 m/s), thin and dense basal layer overlain by a thicker more dilute and slower current. And between the two layers there was a steep concentration gradient (Figure 10). Then the 11 minutes lag between CT-derived maximum concentration and peak ADCP backscatter can be interpreted as follows. About 2 minutes after the arrival of the turbidity current, the thickness of the dilute flow had already reached 20 m. Although the flow was relatively slow at 10 m above the seafloor, the sediment trap package (trap, CT and OBS) was pulled down to the faster flowing layers until the CT sensor at the bottom of the package reached a region just above the dense layer. In this case, the CT sensor recorded the increase in sediment concentration (Figure 5A, Figure 10). Shortly after recording the peak concentration of 12% (minute 11), the CT sensor was clogged at minute 12. It appears that, at this moment, the CT sensor was dipped into the dense layer or even touched the seafloor because of the bedform migration. The CT sensor probably stayed clogged even after rising above the dense layer when the flow began to slow down and the mooring returned upright (Figure 10).

The dense near bed layer of the January 15 flow can thus be several meters thick (Figure 10), which is consistent with the conceptual model proposed by Paul et al. (2018) and Heerema et al. (2020) that a fast and dense basal layer exists at the flow front, which drives the diluted flow above it. Future work is now needed, but also a challenge, to figure out the actual type of the basal layer, be it a high-density turbidity current (Talling et al., 2012) or special thick bedload layer which is only a few grains thick in rivers (van Rijn, 1984), such as by identifying

the deposits form the turbidity current, or via detailed measurements of sediment concentration by ADCP.

5 Conclusions

The 15 January 2016 turbidity current in Monterey Canyon possessed a dense basal layer overlain by a thicker (~50 m) dilute flow. At the interface of these two layers, there seems to be a sharp steep concentration gradient. The maximum sediment concentration in the dense basal layer, measured by a novel conductivity method, was 12%. Concentrations deeper into this layer could have been even higher. The temporal duration and longitudinal length of this dense basal layer remains unknown.

The basal layer's presence is consistent with reports of movement of heavy objects at high speeds (Paull et al., 2018), but concentration as high as 12% is the first ever measurement inside the basal layer of field-scale turbidity currents. Understanding whether turbidity currents are entirely dilute and fully turbulent or contain a dilute cloud overlying a thin dense basal layer is critically important because the two types of flows behave in fundamentally different ways, and present very different hazards to seabed structures. Our study also shows how super-high concentrations in basal layer can be successfully measured, thereby provides the necessary means to test turbidity currents models.

Acknowledgments

The Coordinated Canyon Experiment (CCE) project was co-funded by the Natural Environmental Research Council (UK), Monterey Bay Aquarium Research Institute (US), and Ocean University of China. With the support from NSFC projects (grant numbers 41476070, 41530966, 41720104001), Mr. Chenghao Wang and Miss Yueming Wang assisted the laboratory

experiment, data acquisition, and sample analyses. The authors thank Ben Kneller for his encouragement and insightful comments that helped to improve the manuscript. The contribution from all CCE team members, and R/V Western Flyer and R/V Rachel Carson crews, are gratefully acknowledged. The CCE data can be accessed via the database (http://www.marine-geo.org/tools/search/Files.php?data_set_uid=24762).

References

- Archie, G.E. (1942), The electrical resistivity log as an aid in determining some reservoir characteristics, Transactions of the American Institute of Mining and Metallurgical Engineers, v. 146, p. 54-62, doi:10.2118/942054-G.
- Bornhold, B.D., Ren, P., and Prior, D.B. (1994), High-frequency turbidity currents in British Columbia fjords, Geo-Marine Letters, v. 14, no. 4, p. 238–243, doi: 10.1007/BF01274059.
- Bowen, A. J., Normark, W. R., and Piper, D. J. W. (1984), Modelling of turbidity currents on Navy Submarine Fan, California Continental Borderland: Sedimentology, v. 31, no. 2, p. 169-185, doi: 10.1111/j.1365-3091.1984.tb01957.x.
- Catharina J. Heerema, Peter J. Talling, Matthieu J. Cartigny, Charles K. Paull, Lewis Bailey, Stephen M. Simmons, Daniel R. Parsons, Michael A. Clare, Roberto Gwiazda, Eve Lundsten, Krystle Anderson, Katherine L. Maier, Jingping P. Xu, Esther J. Sumner, Kurt Rosenberger, Jenny Gales, Mary McGann, Lionel Carter, Edward Pope (2020), What determines the downstream evolution of turbidity currents?, Earth and Planetary Science Letters, Volume 532, doi: 10.1016/j.epsl.2019.116023.

- Clare, M.A., Cartigny, M.J.B., North, L.J., Talling, P.J., Vardy, M.E., Hizzett, J.L., Sumner, E.J.,
Hughes Clarke, J.E., Fugro, B., and Cooper, C.C. (2015), Quantification of near-bed
dense layers and implications for seafloor structures: New insights into the most
hazardous aspects of turbidity currents, in Proceedings Offshore Technology Conference
2015, p. 4-7, doi:10.4043/25705-MS.
- Dai, Q., Shan, H. X., Cui, W. L., and Jia, Y. G. (2011), A laboratory study on the relationships
between suspended sediment content and the conductivity and their influencing factors
[in Chinese with English abstract], *Acta Oceanologica Sinica*, v. 33, no. 4, p. 88-94.
- Garcia, M., and Parker, G. (1993), Experiments on the entrainment of sediment into suspension
by a dense bottom current, *Journal of Geophysical Research Oceans*, v. 98, no. C3, p.
4793-4807, doi:10.1029/92JC02404.
- Gartner, J.W. (2004), Estimating suspended solids concentrations from backscatter intensity
measured by acoustic Doppler current profiler in San Francisco Bay, California, *Marine
Geology*, v. 211, no. 3, p. 169-187, doi:10.1016/j.margeo.2004.07.001.
- Ha, H.K., Maa, J.P.Y., Park, K., and Kim, Y.H. (2011), Estimation of high-resolution sediment
concentration profiles in bottom boundary layer using pulse-coherent acoustic Doppler
current profilers, *Marine Geology*, v. 279, no. 1, p. 199-209, doi:
10.1016/j.margeo.2010.11.002.
- Hughes Clarke, J. E. (2016), First wide-angle view of channelized turbidity currents links
migrating cyclic steps to flow characteristics, *Nature Communications*, v. 7, p. 11896,
doi:10.1038/ncomms11896 (2016).

441 Jackson, P. D., Smith, D. T., and Stanford, P. N. (1978), Resistivity-porosity-particle shape
 442 relationships for marine sands, *Geophysics*, v. 43, no. 6, p. 1250-1268, doi:
 443 10.1190/1.1440891.

444 Kneller, B.C., and Branney, M.J. (1995), Sustained high-density turbidity currents and the
 445 deposition of thick massive sands, *Sedimentology*, v. 42, no. 4, p. 607-616, doi:
 446 10.1111/j.1365-3091.1995.tb00395.x.

447 Kuenen, P.H., and Migliorini, C.I. (1950), Turbidity currents as a cause of graded bedding,
 448 *Journal of Geology*, v. 58, no. 2, p. 91-127, doi:10.1086/625710.

449 Leclair, S.F. and Arnott, R.W.C. (2003), Coarse-tail graded, structureless strata: indicators of an
 450 internal hydraulic jump. In: *Shelf Margin Deltas and Linked Down Slope Petroleum*
 451 *Systems: Global Significance and Future Exploration Potential* (Eds H.H. Roberts, N.C.
 452 Rosen, R.H. Filion, and J.B. Anderson), SEPM, Gulf Coast Section, Houston, p. 817–
 453 836.

454 Light, T.S., McHale, E. J., and Fletcher, K. S. (1989), Electrodeless conductivity, *Talanta*, v. 36,
 455 no. 1, p. 235-241, doi:10.1016/0039-9140(89)80101-8.

456 Lowe, D.R. (1982), Sediment gravity flows: II. Depositional models with special reference to the
 457 deposits of high-density turbidity currents, *Journal of Sedimentary Research*, v. 52, no. 6,
 458 p. 343-361, doi:10.1306/212F7F31-2B24-11D7-8648000102C1865D.

459 Maier, K. L., Gales, J. A., Paull, C. K., Rosenberger, K., Talling, P. J., Simmons, S. M.,
 460 Gwiazda, R., McGann, M., Cartigny, M. J. B., Lundsten, E., Anderson, K., Clare, M. A.,
 461 Xu, J., Parsons, D., Barry, J. P., Wolfson-Schwehr, M., Nieminski, N. M., and Sumner,

- E. J. (2019), Linking Direct Measurements of Turbidity Currents to Submarine Canyon-Floor Deposits: *Frontiers in Earth Science*, v. 7, no. 144.
- Middleton, G.V. (1967), Experiments on density and turbidity currents: III. deposition of sediment, *Canadian Journal of Earth Sciences*, v. 4, no. 3, p. 475-505, doi:10.1139/e67-025.
- Middleton, G.V. (1969), Grain flows and other mass movements down slopes, in Stanley, D.J., ed., *The New Concepts of Continental Margin Sedimentation*, American Geological Institute, Short Course Lecture Notes, p. 1–14.
- Middleton, G.V. (1993), Sediment deposition from turbidity currents, *Annual Review of Earth & Planetary Sciences*, v. 21, no. 1, p. 89-114, doi:10.1146/annurev.ea.21.050193.000513.
- Mulder, T., and Alexander, J. (2001), Abrupt change in slope causes variation in the deposit thickness of concentrated particle-driven density currents, *Marine Geology*, v. 175, no. 1, p. 221-235, doi:10.1016/S0025-3227(01)00114-1.
- Paull, C. K., Talling, P. J., Maier, K. L., Parsons, D., Xu, J., Caress, D. W., et al. (2018), Powerful turbidity currents driven by dense basal layers, *Nature Communications*, v. 9, no. 1, p. 4114, doi:10.1594/IEDA/324529.
- Poisson, A. (1980), Conductivity/salinity/temperature relationship of diluted and concentrated standard seawater, *IEEE Journal of Oceanic Engineering*, v. OE-5, no. 1, p. 41-50, doi:10.1109/JOE.1980.1145442.
- Postma, G., Nemec, W., and Kleinspehn, K.L. (1988), Large floating clasts in turbidites: a mechanism for their emplacement, *Sedimentary Geology*, v. 58, no. 1, p. 47-61, doi:10.1016/0037-0738(88)90005-X.

- Sanders, J.E. (1965), Primary sedimentary structures formed by turbidity currents and related
resedimentation mechanisms, Special Publications, p. 192-219.
- Shen, C., and Lemmin, U. (1996), Ultrasonic measurements of suspended sediments: a
concentration profiling system with attenuation compensation, Measurement Science &
Technology, v. 7, no. 9, p. 1191, doi:10.1088/0957-0233/7/9/001.
- Symons, W.O., Sumner, E.J., Paull, C.K., Cartigny, M.J.B., Xu, J.P., Maier, K.L., Lorenson,
T.D., and Talling, P.J. (2017), A new model for turbidity current behavior based on
integration of flow monitoring and precision coring in a submarine canyon, Geology,
45(4) :367~370, doi:10.1130/G38764.1.
- Stevenson, C. J., Feldens, P., Georgiopoulou, A., Schönke, M., Krastel, S., Piper, D. J. W.,
Lindhorst, K., and Mosher, D. (2018), Reconstructing the sediment concentration of a
giant submarine gravity flow: Nature Communications, v. 9, no. 1, p. 2616.
- Talling, P.J., Masson, D.G., Sumner, E.J., and Malgesini, G. (2012), Subaqueous sediment
density flows: Depositional processes and deposit types, Sedimentology, v. 59, no. 7, p.
1937–2003, doi:10.1111/j.1365-3091.2012.01353.x.
- Talling, P.J., et al. (2015), Key future directions for research on turbidity currents and their
deposits, Journal of Sedimentary Research, v. 85, no. 2, p. 153-169, doi:
10.2110/jsr.2015.03.
- Thorne, P. D., Hardcastle, P. J., and Soulsby, R. L. (1993), Analysis of Acoustic Measurements
of Suspended Sediment, Journal of Geophysical Research C, v. 98, no. C1, p. 899-910,
doi:10.1029/92JC01855.

505 Traykovski, P., Geyer, W.R., Irish, J.D., and Lynch, J.F. (2000), The role of wave-induced
 506 density-driven fluid mud flows for cross-shelf transport on the Eel River continental
 507 shelf, *Continental Shelf Research*, v. 20, no. 16, p. 2113-2140, doi:10.1016/S0278-
 508 4343(00)00071-6.

509 van Rijn, L. C. (1984), Sediment transport, Part I: bed load transport. *J. Hydraul. Eng.* 110,
 510 1431–1456.

511 Xu, J.P., Noble, M.A., and Rosenfeld, L.K. (2004), In-situ measurements of velocity structure
 512 within turbidity currents, *Geophysical Research Letters*, v. 31, no. 9, p. 9311, doi:
 513 10.1029/2004GL019718.

514 Xu, J.P., Sequeiros, O.E., and Noble, M.A. (2014), Sediment concentrations, flow conditions,
 515 and downstream evolution of two turbidity currents, Monterey Canyon, USA, *Deep Sea*
 516 *Research Part I Oceanographic Research Papers*, v. 89, no. 3, p. 11-34, doi:
 517 10.1016/j.dsr.2014.04.001.

518 Zhao, L., Ouillon, R., Vowinckel, B., Meiburg, E., Kneller, B., and He, Z. (2018), Transition of a
 519 hyperpycnal flow into a saline turbidity current due to differential diffusivities,
 520 *Geophysical Research Letters*, v. 45, no. 21, p. 11,875-811,884, doi:
 521 10.1029/2018GL080150.